

Safety-Certificated Line-of-Sight Guidance of Unmanned Surface Vehicles for Straight-Line Following in a Constrained Water Region Subject to Ocean Currents

Zhouhua Peng^{1,2}, Jianzhong Li^{1,2}, Bing Han^{3,4} and Nan Gu^{1,2}

Received: 20 June 2022 / Accepted: 08 January 2023

© Harbin Engineering University and Springer-Verlag GmbH Germany, part of Springer Nature 2023

Abstract

The collision-free straight-line following of an unmanned surface vehicle (USV) moving in a constrained water region subject to stationary and moving obstacles is addressed in this paper. USV systems are normally subjected to surge velocity constraints, yaw rate constraints, and unknown ocean currents. Herein, a safety-certificated line-of-sight (LOS) guidance method is proposed to achieve a constrained straight-line following task. First, an antidisturbance LOS guidance law is designed based on the LOS guidance scheme and an extended state observer. Furthermore, collision avoidance with waterway boundaries and stationary/moving obstacles is encoded in control barrier functions, utilizing which the safety constraints are transformed into input constraints. Finally, safety-certificated guidance signals are obtained by solving a quadratic programming problem subject to input constraints. Using the proposed safety-certified LOS guidance method, the USV can accomplish a straight-line following task with guaranteed input-to-state safety. Simulation results substantiate the efficacy of the proposed safety-certificated LOS guidance method for the straight-line following of USVs moving in a constrained water region subject to unknown ocean currents.

Keywords Line-of-sight guidance; Constrained water region; Unmanned surface vehicle; Control barrier function; Extended state observer

1 Introduction

Water transport plays an important role in economic developments and accounts for about 95% of global transpor-

tation tasks (Gu et al., 2023; Zereik et al., 2018; Wu et al., 2020; Campbell et al., 2012; Peng et al., 2021; Lv et al., 2022; Zhang et al., 2018; Wang et al., 2021). Unmanned surface vehicles (USVs) are versatile watercraft that can perform water transportation tasks with minimum human supervision (Li et al., 2022; Shi et al., 2017; Skjetne et al., 2005; Gu et al., 2021; Chen and Wei, 2014; Wu et al., 2021; Veremey, 2014; Wu et al., 2022a; Ma et al., 2018). Trajectory tracking and path following are two fundamental motion control problems for USVs (Qu et al., 2017; Aguiar and Hespanha, 2007; Paliotta et al., 2019; Jiang and Liang, 2018; Ma et al., 2022). In particular, trajectory tracking requires a USV to track a time-related trajectory (Peng et al., 2021; Yu et al., 2020; Katayama and Aoki, 2014; He et al., 2017; Li et al., 2018), whereas path following refers to forcing a USV to follow a path without strict temporal specifications. Path following takes an attractive decoupling property between the geometric task of controlling the USV position and the dynamic task of assigning a speed profile for virtual tracking (Wang et al., 2012; Meng et al., 2012; Deng et al., 2020; Abdurahman et al., 2019; Breivik et al., 2008; Wang et al., 2019; Fossen et al., 2017; Qu et al., 2017; Ma et al., 2021; Wu et al., 2022b; Peng et al., 2023).

Article Highlights

- A CBF-based safe-certificated LOS guidance method is proposed to address the guidance problem in a constrained water region.
- The proposed guidance method can address the collision avoidance with stationary/moving obstacles, in addition to the waterway boundaries.
- An optimization-based guidance method is proposed to guarantee the guidance law satisfying the input constraints in the path following task.

✉ Nan Gu
ngu@dlmu.edu.cn

¹ School of Marine Electrical Engineering, Dalian Maritime University, Dalian 116026, China

² Dalian Key Laboratory of Swarm Control and Electrical Technology for Intelligent Ships, Dalian 116026, China

³ Shanghai Ship and Shipping Research Institute Co. Ltd., Shanghai 200135, China

⁴ National Engineering Research Center of Ship & Shipping Control System, Shanghai 200135, China

In recent years, line-of-sight (LOS) guidance, as an intuitive and effective way to achieve path convergence, has been studied on the basis of path following. In Fossen and Pettersen (2014), a proportional LOS guidance law is proposed, and its uniform semi-global exponential stability is proven. In Caharijia et al. (2016), an integral LOS guidance law is constructed to compensate for the drift effect of environmental disturbances. In the study conducted by Belleter et al. (2019), an adaptive LOS guidance law is proposed to solve the problem of path following subject to constant ocean currents. In Liu et al. (2017), an extended state observer (ESO)-based LOS guidance law is proposed, where a reduced-order ESO is used to estimate the time-varying sideslip angle. Moreover, two ESOs are used to separately estimate surge and sway linear velocities (Yu et al., 2019a); that is, the unmeasured sideslip angle can be indirectly calculated and compensated on the basis of the LOS guidance law. In Yu et al. (2019b), a finite-time LOS-based guidance law is developed; that is, path following can be achieved within a finite time. However, the abovementioned LOS guidance methods only consider a USV running in an open-water area. With regard to a USV running in a constrained water region, e.g., inland rivers or canals, the abovementioned LOS guidance methods cannot be applied as safety cannot be ensured. In achieving path following in a constrained water region, an error-constrained LOS guidance law is proposed (Zheng et al., 2018; Zheng, 2020), where the path following tracking errors are constrained by using a tan-type barrier Lyapunov function method. Although the error-constrained LOS guidance method could avoid collisions with waterway boundaries by constraining tracking errors, it cannot address guidance moving in a constrained water region with multiple stationary and moving obstacles.

Given the abovementioned discussions, this paper investigates the safety-certificated LOS guidance of a USV in a constrained water region with multiple obstacles. First, an ESO is proposed to estimate unknown ocean currents. Next, a straight-line LOS guidance law is designed on the basis of the estimated information from the ESO. Then, in achieving a collision-free straight-line following task, control barrier functions (CBFs) are used to optimize the guidance signals where safe guidance signals are obtained by solving a quadratic programming problem. By using the proposed safe-certificated LOS guidance method, the USV can follow a straight-line path in a constrained water region while ensuring safety. Finally, the closed-loop guidance system can ensure input-to-state safety (ISSf) and that all error signals are uniformly and ultimately bounded. Simulation results are provided to substantiate the efficacy of the proposed safe-certificated LOS guidance method for straight-line following of a USV in a constrained water region.

- In contrast to the LOS guidance method proposed by Fossen and Pettersen (2014), Caharijia et al. (2016), Liu et al. (2016), Liu et al. (2017), Belleter et al. (2019), Yu et al. (2019a), Yu et al. (2019b), and Peng et al. (2019), which lacks environmental constraints, a CBF-based safe-certificated LOS guidance method is proposed herein to address the guidance problem in a constrained water region with waterway boundaries. The proposed safe-certificated LOS guidance law can prevent collisions between the USV and waterway boundaries, allowing the USV to safely navigate through narrow waterways.

- In contrast to the error-constrained LOS guidance method (Zheng et al., 2018; Zheng, 2020), where the tracking errors are confined without violating waterway constraints, the proposed guidance method can address the collision avoidance problem with multiple stationary and moving obstacles in the constrained water region, in addition to the waterway boundaries.

- In contrast to the LOS guidance method proposed by Fossen and Pettersen (2014), Caharijia et al. (2016), Liu et al. (2017), Belleter et al. (2019), Yu et al. (2019a), Yu et al. (2019b), Zheng et al. (2018), and Zheng (2020) where the input constraints are not considered, an optimization-based guidance method is proposed to ensure that the resulting guidance law satisfies the input constraints in path following and collision avoidance tasks.

2 Preliminaries and problem formulation

2.1 Notation

\mathbb{R}^n denotes the n -dimensional Euclidean space. $|\cdot|$ represents the absolute value of a real number. $\|\cdot\|$ denotes the two-norm of a matrix or a vector. I_n denotes an identity matrix with n dimension. A continuous function $\gamma: [b, a) \rightarrow \mathbb{R}^+$ with $\gamma(0) = 0$ and γ is strictly and monotonically increasing. If $a \in \mathbb{R}^+$ and $b = 0$, then γ is a class \mathcal{K} function. If $a = \infty$, $b = 0$ and $\lim_{x \rightarrow \infty} \gamma(x) = \infty$, then γ is a class \mathcal{K}_∞ function. If $\gamma: \mathbb{R} \rightarrow \mathbb{R}$, $\lim_{x \rightarrow \infty} \gamma(x) = \infty$, and $\lim_{x \rightarrow -\infty} \gamma(x) = -\infty$, then γ is a class extended \mathcal{K}_∞ function denoted by $\mathcal{K}_{\infty,e}$.

2.2 Control barrier function

Consider the following continuous time dynamical systems,

$$\dot{\mathbf{x}} = \mathbf{f}(\mathbf{x}) + \mathbf{g}(\mathbf{x})\mathbf{u} \quad (1)$$

$$\dot{\mathbf{x}} = \mathbf{f}(\mathbf{x}) + \mathbf{g}(\mathbf{x})(\mathbf{u} + \mathbf{w}) \quad (2)$$

where $\mathbf{x} \in \mathbb{R}^n$ is the state; $\mathbf{u} \in \mathbb{R}^m$ is the control input; $\mathbf{w} \in \mathbb{R}^m$ is the disturbance assumed to be bounded and satisfied $\|\mathbf{w}\|_\infty \triangleq \text{ess sup}_{t > 0} \|\mathbf{w}\|$. The function $\mathbf{f}: \mathbb{R}^n \rightarrow \mathbb{R}^n$

and $g: \mathbb{R}^n \rightarrow \mathbb{R}^{n \times m}$ are continuously differentiable.

Let $h: \mathbb{R}^n \rightarrow \mathbb{R}$ be a continuously differentiable function. Consider a set $\mathcal{S} \subset \mathbb{R}^n$, the 0-superlevel set of h is defined as follows:

$$\begin{aligned}\mathcal{S} &= \{ \mathbf{x} \in \mathbb{R}^n | h(\mathbf{x}) \geq 0 \} \\ \partial \mathcal{S} &= \{ \mathbf{x} \in \mathbb{R}^n | h(\mathbf{x}) = 0 \} \\ \text{Int}(\mathcal{S}) &= \{ \mathbf{x} \in \mathbb{R}^n | h(\mathbf{x}) > 0 \}\end{aligned}\quad (3)$$

For any $\mathbf{x}(0) \in \mathcal{S}$, $\mathbf{x}(t) \in \mathcal{S}$ with $t \in [0, T_{\max})$, set \mathcal{S} is called forward invariant, and when $T_{\max} = \infty$, it is called forward complete (Molnar et al., 2022). The nominal closed-loop system (1) is safe on set \mathcal{S} if \mathcal{S} is forward invariant.

Definition 1 (Ames et al., 2017). Let $\mathcal{S} \subset \mathbb{R}^n$ be the 0-superlevel set of a continuously differentiable function $h: \mathbb{R}^n \rightarrow \mathbb{R}$ given in (3). Then, $h(\mathbf{x})$ is a CBF for the system (1) on \mathcal{S} if there exists $\alpha \in \mathcal{K}_{\infty, e}$ such that $\forall \mathbf{x} \in \mathcal{S}$.

$$\sup_{\mathbf{u} \in \mathbb{R}^m} \dot{h}(\mathbf{x}, \mathbf{u}) \triangleq L_f h(\mathbf{x}) + L_g h(\mathbf{x}) \mathbf{u} \geq -\alpha(h(\mathbf{x})) \quad (4)$$

where $L_f h$ and $L_g h$ represent the Lie derivatives of $h(\mathbf{x})$.

Definition 2 (Kolathaya and Ames, 2019). Let $\mathcal{S} \subset \mathbb{R}^n$ be the 0-superlevel set of a continuously differentiable function $h: \mathbb{R}^n \rightarrow \mathbb{R}$. Then, $h(\mathbf{x})$ is an ISSf-CBF for the disturbed system (2) on set \mathcal{S} if there exists $\alpha \in \mathcal{K}_{\infty, e}$, $\iota \in \mathcal{K}_{\infty}$ such that $\forall \mathbf{x} \in \mathcal{S}$.

$$\sup_{\mathbf{u} \in \mathbb{R}^m} L_f h(\mathbf{x}) + L_g h(\mathbf{x}) \mathbf{u} \geq -\alpha(h(\mathbf{x})) - \iota(\|\mathbf{w}\|_{\infty}) \quad (5)$$

Lemma 1 (Das and Richard, 2022). Consider the disturbed system (2) with an estimated error quantified by an observer that provides $\hat{\mathbf{w}}$ with an estimation error bound $\|L_g h(\mathbf{x}) \hat{\mathbf{w}}\| \leq M_d$. A continuous differentiable function $h: \mathbb{R}^n \rightarrow \mathbb{R}$ and $\gamma \in \mathcal{K}_{\infty, e}$ are given for the nominal system (1). If a control signal $\mathbf{u} \in \mathbb{R}^m$ is satisfied, then a robust CBF constraint is defined as follows:

$$L_f h(\mathbf{x}) + L_g h(\mathbf{x}) (\mathbf{u} + \hat{\mathbf{w}}) - M_d \geq -\alpha(h(\mathbf{x})) \quad (6)$$

Lemma 1 applies to high-relative-degree CBF constraints. The d th-order time derivative of $h(\mathbf{x})$ is given as follows:

$$h^d(\mathbf{x}, \mathbf{u}, \mathbf{w}) = L_f^d h(\mathbf{x}) + L_g L_f^{d-1} h(\mathbf{x}) (\mathbf{u} + \mathbf{w}) \quad (7)$$

where the unknown dynamics $L_g L_f^{d-1} h(\mathbf{x}) \mathbf{w}$ can be estimated by an observer. If there exists a constant $M_e \in \mathbb{R}^+$ such that the estimation error $\|L_g L_f^{d-1} h(\mathbf{x}) \hat{\mathbf{w}}\| \leq M_e$, then the robust CBF constraint is defined as follows:

$$L_f^d h(\mathbf{x}) + L_g L_f^{d-1} h(\mathbf{x}) (\mathbf{u} + \hat{\mathbf{w}}) - M_e \geq -K_a \boldsymbol{\eta}_b(\mathbf{x}) \quad (8)$$

where $\boldsymbol{\eta}_b(\mathbf{x}) = [h(\mathbf{x}), \dot{h}(\mathbf{x}), \ddot{h}(\mathbf{x}), \dots, h^{d-1}(\mathbf{x})]^T$ and $K_a \in \mathbb{R}^d$.

2.3 Problem Formulation

Two reference frames are used to describe the motion of a USV: an earth-fixed frame and a body-fixed frame. The kinematics of the USV is expressed as follows:

$$\dot{\boldsymbol{\eta}} = \mathbf{R}(\psi) \begin{pmatrix} u \\ v \\ r \end{pmatrix} + \mathbf{R}(\psi_{id}) \begin{pmatrix} w_s \\ w_e \\ 0 \end{pmatrix} \quad (9)$$

where $\boldsymbol{\eta} = [p^T, \psi]^T \in \mathbb{R}^3$ with $\mathbf{p} = [x, y]^T \in \mathbb{R}^2$ denotes the position, and $\psi \in (-\pi, \pi]$ denotes the yaw angle; u , v , and $r \in \mathbb{R}$ indicate the surge velocity, sway velocity, and yaw rate in the body-fixed frame, respectively; $\psi_{id} \in (-\pi, \pi]$ denotes the i th route segment. w_s and w_e denote constant disturbance induced by ocean currents; $\mathbf{R}(\psi)$ and $\mathbf{R}(\psi_{id})$ are rotation matrixes defined as follows:

$$\mathbf{R}(\psi) = \begin{bmatrix} \cos(\psi) & -\sin(\psi) & 0 \\ \sin(\psi) & \cos(\psi) & 0 \\ 0 & 0 & 1 \end{bmatrix} \quad (10)$$

As shown in Figure 1, a sequence of the desired straight-line route segments is defined as follows:

$$a_i x_{id} + b_i y_{id} + c_i = 0 \quad (11)$$

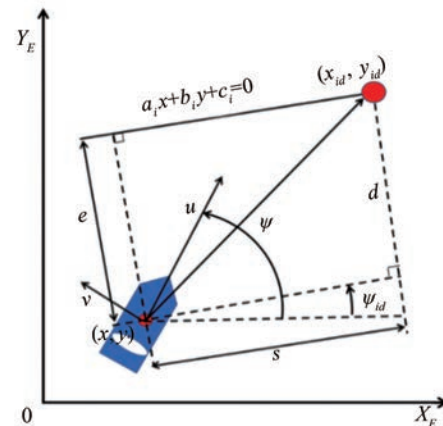


Figure 1 USV model

where a_i , b_i , and $c_i \in \mathbb{R}$ are the parameters; subscript i denotes the i th route segment. The waypoint $\mathbf{p}_{id} = [x_{id}, y_{id}]^T \in \mathbb{R}^2$ on the route is obtained as follows:

$$a_i x_{id} + b_i y_{id} + c_i = 0 \quad (12)$$

In accomplishing the straight-line following task, waypoint tracking errors are defined as follows:

$$\begin{pmatrix} s \\ e \end{pmatrix} = \mathbf{R}^T(\psi_{id}) \begin{pmatrix} x - x_{id} \\ y - y_{id} \end{pmatrix} \quad (13)$$

The time derivative of Equation (13) along the kinematics (9) is given as follows:

$$\begin{pmatrix} \dot{s} \\ \dot{e} \end{pmatrix} = \begin{bmatrix} U \cos(\psi - \psi_{id} + \beta) + w_s \\ U \sin(\psi - \psi_{id} + \beta) + w_e \end{bmatrix} \quad (14)$$

where $\beta = \text{atan}(v/u)$ denotes the sideslip angle; $\psi_{id} = \text{atan2}(-a_i, b_i)$ and $U = \sqrt{u^2 + v^2}$ are the resultant velocity.

As shown in Figure 2, the constrained water region can be modeled as two waterway boundaries $L_{ij}, j = 1, 2$ parallel to the i th straight-line route segment. The two waterway boundaries are $L_{ij} = \{a_{ij}, b_{ij}, c_{ij} \in \mathbb{R} | a_{ij}x + b_{ij}y + c_{ij} = 0, i = 1, 2, \dots, n, j = 1, 2\}$. Next, consider M_1 static obstacles $O_{ks}, k = 1, 2, \dots, M_1$, which are modeled as a closed circular disk of radius d_{ks} , centered at $p_{ks} = [x_{ks}, y_{ks}]^T \in \mathbb{R}^2$. Consider M_2 moving obstacles $O_{km}, k = 1, 2, \dots, M_2$, which is modeled as a closed circular disk of radius d_{km} , centered at $p_{km} = [x_{km}, y_{km}]^T \in \mathbb{R}^2$.

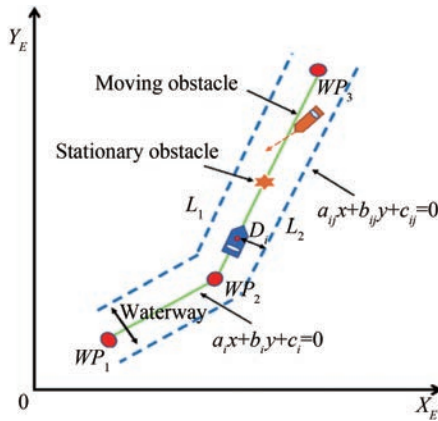


Figure 2 Straight-line following of a USV in the constrained water region

The safe-certificated straight-line following in a constrained water region aims to design a guidance method for a USV with kinematics (9); that is, the USV is able to converge to the straight-line path and avoid collisions with waterway boundaries and stationary/moving obstacles. In particular, the control objective is divided into four parts.

- The goal reaching task is achieved as follows:

$$\lim_{t \rightarrow \infty} \|p - p_{id}\| \leq \varepsilon_0 \quad (15)$$

where $\varepsilon_0 \in \mathbb{R}$ is a small positive constant.

- Collision avoidance with a waterway boundary task is measured as follows:

$$D_{ij} - \sqrt{L^2 + W^2}/2 > d_{ij}, \quad i = 1, 2, \dots, n, \quad j = 1, 2 \quad (16)$$

where D_{ij} is the distance between USV's center point and the waterway boundary; L is the length of the USV; W is the width of the USV; $d_{ij} \in \mathbb{R}$ denotes the safe distance between the waterway boundary and the USV.

- Collision avoidance with a stationary obstacle task is measured as follows:

$$\|p - p_{ks}\| > d_{ks}, \quad k = 1, 2, \dots, M_1 \quad (17)$$

where $d_{ks} \in \mathbb{R}$ denotes the safe distance between the stationary obstacles and the USV.

- Collision avoidance with a moving obstacle task is calculated as follows:

$$\|p - p_{km}\| > d_{km}, \quad k = 1, 2, \dots, M_2 \quad (18)$$

where $d_{km} \in \mathbb{R}$ denotes the safe distance between the moving obstacle and the USV.

3 Design and analysis

As shown in Figure 3 a safety-certificated LOS guidance is designed in this section. First, a straight-line LOS guidance law is developed where an ESO is used to estimate unknown ocean currents. Next, CBFs are constructed to encode currents' collision avoidance tasks of waterway boundaries and stationary/moving obstacles as safety constraints. Finally, quadratic programming problems are formulated to obtain safety-certificated guidance signals within safety and velocity constraints.

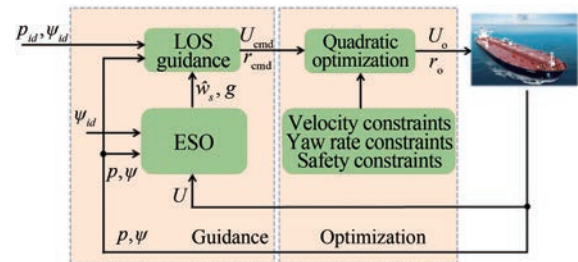


Figure 3 Safety-certificated LOS guidance structure

3.1 Ocean current ESO design

Let \hat{w}_s and \hat{w}_e be the estimates of w_s and w_e , respectively. A linear ESO is developed to estimate the unknown ocean as follows:

$$\begin{bmatrix} \dot{\hat{s}} \\ \dot{\hat{e}} \\ \dot{\hat{w}}_s \\ \dot{\hat{w}}_e \end{bmatrix} = \begin{bmatrix} U \cos(\psi - \psi_{id} + \beta) + \hat{w}_s - k_{s1}\tilde{s} \\ U \sin(\psi - \psi_{id} + \beta) + \hat{w}_e - k_{e1}\tilde{e} \\ -k_{s2}\tilde{s} \\ -k_{e2}\tilde{e} \end{bmatrix} \quad (19)$$

where $\tilde{s} = \hat{s} - s$ and $\tilde{e} = \hat{e} - e$; k_{s1} , k_{e1} , k_{s2} , and $k_{e2} \in \mathfrak{R}$ are positive gains.

Let $\tilde{w}_s = \hat{w}_s - w_s$ and $\tilde{w}_e = \hat{w}_e - w_e$. Consequently, the estimation error dynamics is given as follows:

$$\dot{\mathbf{E}}_1 = \mathbf{A}\mathbf{E}_1 + \mathbf{B}\mathbf{w} \quad (20)$$

where $\mathbf{E}_1 = [\tilde{s}, \tilde{e}, \tilde{w}_s, \tilde{w}_e]^T$, $\mathbf{w} = [\dot{w}_s, \dot{w}_e]^T$ and

$$\mathbf{A} = \begin{bmatrix} -k_{s1} & 0 & 1 & 0 \\ 0 & -k_{e1} & 0 & 1 \\ -k_{s2} & 0 & 0 & 0 \\ 0 & -k_{e2} & 0 & 0 \end{bmatrix}, \quad \mathbf{B} = \begin{bmatrix} 0 & 0 \\ 0 & 0 \\ -1 & 0 \\ 0 & -1 \end{bmatrix}.$$

Considering that \mathbf{A} is a Hurwitz matrix, a symmetric positive definite matrix \mathbf{P} is observed; that is, $\mathbf{A}^T \mathbf{P} + \mathbf{P}\mathbf{A} = -\zeta \mathbf{I}_4$, where $\zeta \in \mathfrak{R}$ is a positive constant. In analyzing the stability of (20), the following assumption is made (Gu et al., 2022).

Assumption 1. The disturbances' w_i , $i = s, e$ derivatives are bounded; that is, $|\dot{w}_i(t)| + |\ddot{w}_i(t)| < w_i^*$, with w_i^* being a positive constant.

Lemma 2. Under Assumption 1, the ESO subsystem (20), with the state vector being \mathbf{E}_1 and the input being \mathbf{w} , is input-to-state stable (ISS).

Proof: Consider a Lyapunov function

$$V_1 = \frac{1}{2} \mathbf{E}_1^T \mathbf{P} \mathbf{E}_1 \quad (21)$$

and its time derivative along (20) is given as follows:

$$\dot{V}_1 \leq -\frac{\zeta}{2} \|\mathbf{E}_1\|^2 + \|\mathbf{E}_1\| \|\mathbf{P}\mathbf{B}\| \|\mathbf{w}\| \quad (22)$$

As

$$\|\mathbf{E}_1\| \geq 2 \|\mathbf{P}\mathbf{B}\| \|\mathbf{w}\| / (\zeta \theta_1) \quad (23)$$

renders

$$\dot{V}_1 \leq -\frac{\zeta}{2} (1 - \theta_1) \|\mathbf{E}_1\|^2 \quad (24)$$

where $0 < \theta_1 < 1$. Therefore, subsystem (20) is ISS (Khalil, 2015), and $\mathbf{E}_1(t)$ is satisfied as follows:

$$\|\mathbf{E}_1(t)\| \leq \sqrt{\frac{\lambda_{\max}(\mathbf{P})}{\lambda_{\min}(\mathbf{P})}} \max \{ \|\mathbf{E}_1(t_0)\| e^{-\frac{\zeta(1-\theta_1)(t-t_0)}{\lambda_{\max}(\mathbf{P})}}, 2 \|\mathbf{P}\mathbf{B}\| \|\mathbf{w}\| / (\zeta \theta_1) \} \quad (25)$$

3.2 LOS guidance design

Before the design, the following assumption is made.

Assumption 2. Considering kinematics, the kinetic error is assumed to be 0, that is, $U = U_o$, $r = r_o$, where U_o and r_o

are the optimized surge velocity and yaw rate, respectively. Recalling the error dynamics (14),

$$\begin{cases} \dot{s} = (U_e + U_{\text{cmd}})(1 - 2 \sin^2(\frac{\psi - \psi_{id} + \beta}{2})) + w_s \\ \dot{e} = U_o \sin(\psi_{\text{cmd}} + \psi_e + \beta - \psi_{id}) + w_e \end{cases} \quad (26)$$

where $U_e = U_o - U_{\text{cmd}}$ and $\psi_e = \psi - \psi_{\text{cmd}}$.

By using the estimated information from the ESO (19), a LOS guidance law is designed on the basis of (26).

$$\begin{bmatrix} U_{\text{cmd}} \\ \psi_{\text{cmd}} \\ r_{\text{cmd}} \end{bmatrix} = \begin{bmatrix} -\frac{k_u s}{\sqrt{s^2 + \Delta_u^2}} + f_U - \hat{w}_s \\ \psi_{id} - \arctan\left(\frac{e + g}{\Delta_\psi}\right) - \beta \\ -\frac{k_r \psi_e}{\sqrt{\psi_e^2 + \Delta_r^2}} \end{bmatrix} \quad (27)$$

where $f_U = 2U_o \sin^2(\frac{\psi - \psi_{id} + \beta}{2})$; $k_u > 0$ and $k_r > 0$ are constant controller gains; $\Delta_u > 0$, $\Delta_\psi > 0$ and $\Delta_r > 0$ are parameters. The velocity guidance signal U_{cmd} is designed using feedback linearization. The second term of the heading guidance signal ψ_{cmd} is an LOS angle, which is used to guide the USV converging to the desired path. g is a component additionally designed to compensate for the unknown ocean current in the e direction.

Substituting Equation (27) into Equation (26),

$$\begin{bmatrix} \dot{s} \\ \dot{e} \end{bmatrix} = \begin{bmatrix} -\frac{k_u s}{\sqrt{s^2 + \Delta_u^2}} - \tilde{w}_s + U_e \\ -\frac{U_o(e + g)}{\sqrt{(e + g)^2 + \Delta_\psi^2}} + w_e + G(\cdot) \end{bmatrix} \quad (28)$$

where G is a perturbing term, which is given as follows:

$$\begin{aligned} G(\cdot) &= U_o [1 - \cos(\psi_e)] \sin(\arctan(\frac{e + g}{\Delta_\psi})) \\ &+ U_o \cos(\arctan(\frac{e + g}{\Delta_\psi})) \sin(\psi_e) \end{aligned} \quad (29)$$

$G(\psi_e, \psi_{\text{cmd}}, e, U_o)$ satisfies $G(0, \psi_{\text{cmd}}, e, U_o) = 0$ and $\|G(\cdot)\| \leq \zeta(U_o) \|\psi_e\|$, where $\zeta(U_o) > 0$ (Maghenem et al., 2017). $G(\cdot)$ is zero when the perturbing variable $\tilde{\psi}$ is zero, and it has maximal linear growth in perturbing variables.

In compensating for the ocean current component w_e in (28), g is selected to satisfy the following equality (Belletier et al., 2019):

$$U_o \frac{g}{\sqrt{\Delta_\psi^2 + (e + g)^2}} = \hat{w}_e \quad (30)$$

Based on (30),

$$(U_o^2 - \hat{w}_e^2) \left(\frac{g}{\hat{w}_e} \right)^2 = \Delta_\psi^2 + e^2 + 2e\hat{w}_e \left(\frac{g}{\hat{w}_e} \right) \quad (31)$$

Let $a = \hat{w}_e^2 - U_o^2$, $b = e\hat{w}_e$ and $c = \Delta_\psi^2 + e^2$. Considering that $U_o^2 - \hat{w}_e^2 > 0$, $b^2 - ac = \Delta_\psi^2(U_o^2 - \hat{w}_e^2) + e^2U_o^2 > 0$.

Based on the quadratic formula,

$$g = \hat{w}_e \frac{b + \sqrt{b^2 - ac}}{-a} \quad (32)$$

where the negative root is abandoned to ensure that g and \hat{w}_e have the same sign.

Substituting g into Equation (28), we obtain

$$\begin{bmatrix} \dot{s} \\ \dot{e} \end{bmatrix} = \begin{bmatrix} -\frac{k_u s}{\sqrt{s^2 + \Delta_u^2}} - \tilde{w}_s + U_e \\ -\frac{U_o e}{\sqrt{(e+g)^2 + \Delta_\psi^2}} - \tilde{w}_e + G(\cdot) \end{bmatrix} \quad (33)$$

Lemma 3. The error subsystem (33), viewed as a system with the states being s and e and the inputs being \tilde{w}_s , \tilde{w}_e , U_e , and $G(\cdot)$, is ISS.

Proof: Construct the following Lyapunov function

$$V_2 = \frac{1}{2} s^2 + \frac{1}{2} e^2 \quad (34)$$

and its derivative based on (28) is calculated as follows:

$$\begin{aligned} \dot{V}_2 &= -\bar{k}_u s^2 - \tilde{w}_s s + U_e s - \bar{k}_{U_o} e^2 - \tilde{w}_e e + G(\cdot) e \\ &\leq -\lambda_{\min}(\mathbf{K}) \|\mathbf{E}_2\|^2 + \|h_1\| \|\mathbf{E}_2\| \end{aligned} \quad (35)$$

where $\bar{k}_u = k_u / \sqrt{s^2 + \Delta_u^2}$, $\bar{k}_{U_o} = U_o / \sqrt{(e+g)^2 + \Delta_\psi^2}$, $\mathbf{K} = \text{diag} \{ \bar{k}_u, \bar{k}_{U_o} \}$, $\mathbf{E}_2 = [s, e]^T$, $\mathbf{h}_1 = [|\tilde{w}_s| + |U_e|, |\tilde{w}_e| + |G(\cdot)|]^T$.

As

$$\begin{aligned} \|\mathbf{E}_2\| &\geq \frac{|\tilde{w}_s|}{\theta_2 \lambda_{\min}(\mathbf{K})} + \frac{|U_e|}{\theta_2 \lambda_{\min}(\mathbf{K})} \\ &\quad + \frac{|\tilde{w}_e|}{\theta_2 \lambda_{\min}(\mathbf{K})} + \frac{|G(\cdot)|}{\theta_2 \lambda_{\min}(\mathbf{K})} \\ &\geq \frac{\|\mathbf{h}_1\|}{\theta_2 \lambda_{\min}(\mathbf{K})} \end{aligned} \quad (36)$$

renders

$$\dot{V}_2 \leq -(1 - \theta_2) \lambda_{\min}(\mathbf{K}) \|\mathbf{E}_2\|^2 \quad (37)$$

where $0 < \theta_2 < 1$. Consequently, the error subsystem (28) is ISS, and

$$\|\mathbf{E}_2(t)\| \leq \max \left\{ \|\mathbf{E}_2(0)\| e^{-2\lambda_{\min}(\mathbf{K})(1-\theta_2)(t-t_0)}, \frac{\|\mathbf{h}_1\|}{\theta_2 \lambda_{\min}(\mathbf{K})} \right\} \quad (38)$$

The time derivative of ψ_e is obtained as follows: $\dot{\psi}_e = r - r_{\text{cmd}} + r_{\text{cmd}} - \dot{\psi}_{\text{cmd}}$. By substituting (27) into $\dot{\psi}_e$, the resulting error system can be expressed as follows:

$$\dot{\psi}_e = -\frac{k_r \psi_e}{\sqrt{\psi_e^2 + \Delta_r^2}} + r_e - \dot{\psi}_{\text{cmd}} \quad (39)$$

where $r_e = r_o - r_{\text{cmd}}$.

Lemma 4. The error subsystem (39), viewed as a system with the state being ψ_e and the inputs being r_e and $\dot{\psi}_{\text{cmd}}$, is ISS.

Proof: Construct the following Lyapunov function

$$V_3 = \frac{1}{2} \psi_e^2 \quad (40)$$

and its derivative based on (39) is calculated as follows:

$$\dot{V}_3 = -\bar{k}_r \psi_e^2 + \psi_e r_e - \dot{\psi}_{\text{cmd}} \psi_e \quad (41)$$

where $\bar{k}_r = k_r / \sqrt{\psi_e^2 + \Delta_r^2}$.

As

$$|\psi_e| \geq \frac{|r_e|}{\theta_3 \bar{k}_r} + \frac{|\dot{\psi}_{\text{cmd}}|}{\theta_3 \bar{k}_r} \quad (42)$$

renders

$$\dot{V}_3 \leq -(1 - \theta_3) \bar{k}_r |\psi_e|^2 \quad (43)$$

where $0 < \theta_3 < 1$. Consequently, the error subsystem (39) is ISS, and

$$|\psi_e| \leq \max \left\{ |\psi_e(0)| e^{-2\bar{k}_r(1-\theta_3)(t-t_0)}, \frac{|r_e| + |\dot{\psi}_{\text{cmd}}|}{\theta_3 \bar{k}_r} \right\}$$

Lemma 5. The cascaded system formed by subsystem (20), subsystem (33), and subsystem (39) is ISS.

Proof: Based on Lemmas 2 and 3, the ESO subsystem and error subsystem (33) can be considered a cascade system, with the states being s, e and the input being w , which is ISS. Based on Lemmas 3 and 4, the error subsystems (33) and (39) can be regarded as a cascade system, with the states being s, e and the inputs being $r_e, \dot{\psi}_{\text{cmd}}$, which is ISS. Based on Lemma 4.6 in Khalil (2015), the closed-loop system composed of (20), (33), and (39) is ISS.

3.3 CBF design

In this subsection, the collision avoidance of waterway

boundaries and stationary/moving obstacles is addressed and encoded as safety constraints by CBFs. Then, a quadratic optimization problem is established to optimize the command signals obtained in Section 3.2.

3.3.1 CBF design for avoiding stationary obstacles

Let $\mathbf{p}_{ks} = [x_{ks}, y_{ks}]^T$ be the position of the stationary obstacles. In avoiding the stationary obstacles, the following CBF for the collision avoidance of stationary obstacles is constructed:

$$\mathcal{S}_1 = \{ \mathbf{p} \in \mathbb{R}^2 | h_{ks}(\mathbf{p}, \mathbf{p}_{ks}) = \|\mathbf{p} - \mathbf{p}_{ks}\|^2 - d_{ks}^2 \geq 0 \} \quad (44)$$

Recalling (9), it follows that

$$\dot{\mathbf{p}} = \begin{bmatrix} U_o \cos(\psi + \beta) \\ U_o \sin(\psi + \beta) \end{bmatrix} + \begin{bmatrix} \hat{w}_x \\ \hat{w}_y \end{bmatrix} - \begin{bmatrix} \tilde{w}_x \\ \tilde{w}_y \end{bmatrix} \quad (45)$$

where $[\hat{w}_x, \hat{w}_y]^T = \underline{R}(\psi_{id}) [\hat{w}_s, \hat{w}_e]^T$, $[\tilde{w}_x, \tilde{w}_y]^T = \underline{R}[\tilde{w}_s, \tilde{w}_e]^T$ and

$$\underline{R}(\psi_{id}) = \begin{bmatrix} \cos(\psi_{id}) & -\sin(\psi_{id}) \\ \sin(\psi_{id}) & \cos(\psi_{id}) \end{bmatrix}$$

Using (8), the second time derivatives of h_{ks} in (44) can be expressed as follows:

$$\ddot{h}_{ks} + 2\alpha_s \dot{h}_{ks} + \alpha_s^2 h_{ks} \geq 0, \quad k = 1, 2, \dots, M_1 \quad (46)$$

and the corresponding constraints are expressed as follows:

$$\mathcal{U}_1(r_o) = \{ r_o | A_{ks} r_o + B_{ks} \alpha_s + C_{ks} \alpha_s^2 + M_{ks} \geq D_{ks} \} \quad (47)$$

$$k = 1, 2, \dots, M_1$$

where

$$\begin{aligned} A_{ks} &= -2U_o((x - x_{ks})\sin(\psi + \beta) \\ &\quad - (y - y_{ks})\cos(\psi + \beta)) \\ B_{ks} &= 4U_o((x - x_{ks})\cos(\psi + \beta) + (y - y_{ks})\sin(\psi + \beta)) \\ &\quad + 4(x - x_{ks})\hat{w}_x + 4(y - y_{ks})\hat{w}_y \\ C_{ks} &= (x - x_{ks})^2 + (y - y_{ks})^2 - d_{ks}^2 \\ D_{ks} &= -2\dot{U}_o((x - x_{ks})\cos(\psi + \beta) \\ &\quad + (y - y_{ks})\sin(\psi + \beta)) \\ &\quad - 2(U_o^2 + \hat{w}_x^2 + \hat{w}_y^2 + 2U\hat{w}_x \cos(\psi + \beta) \\ &\quad + 2U_o\hat{w}_y \sin(\psi + \beta)) \\ M_{ks} &= -4\alpha_o(\tilde{w}_x(x - x_{ks}) + \tilde{w}_y(y - y_{ks})) \\ &\quad - 2\tilde{w}_x(2U_o \cos(\psi + \beta) + 2\hat{w}_x - \tilde{w}_x) \\ &\quad - 2\tilde{w}_y(2U_o \sin(\psi + \beta) + 2\hat{w}_y - \tilde{w}_y) \end{aligned}$$

and $\alpha_s \in \mathbb{R}$ is a positive constant.

3.3.2 CBF design for avoiding moving obstacles

In avoiding the moving obstacles, the following CBF is

constructed as follows:

$$\mathcal{S}_2 = \{ \mathbf{p} \in \mathbb{R}^2 | h_{km}(\mathbf{p}, \mathbf{p}_{km}) = \|\mathbf{p} - \mathbf{p}_{km}\|^2 - d_{km}^2 \geq 0 \} \quad (48)$$

Using (8), the time derivatives of h_{km} in (48) can be expressed as follows:

$$\dot{h}_{km}(\mathbf{p}, \mathbf{p}_{km}) \geq -\alpha_m h_j(\mathbf{p}, \mathbf{p}_{km}) \quad (49)$$

and the corresponding constraints are expressed as follows:

$$\mathcal{U}_2(U_o) = \{ U_o | A_{km} U_o + B_{km} \alpha_m + M_{km} \geq D_{km} \} \quad (50)$$

$$k = 1, 2, \dots, M_2$$

where

$$\begin{aligned} A_{km} &= 2(x - x_{km})\cos(\psi + \beta) + 2(y - y_{km})\sin(\psi + \beta) \\ B_{km} &= (x - x_{km})^2 + (y - y_{km})^2 - d_{km}^2 \\ D_{km} &= -2\hat{w}_x(x - x_{km}) - 2\hat{w}_y(y - y_{km}) \\ M_{km} &= -2\tilde{w}_x(x - x_{km}) - 2\tilde{w}_y(y - y_{km}) \end{aligned}$$

and $\alpha_m \in \mathbb{R}$ is a positive constant.

Remark 1: Based on Rule 9(e) of the International Regulations for Preventing Collisions at Sea (COLREGS), in a narrow waterway or fairway, overtaking can only occur if the vessel to be overtaken takes action to permit safe passing. Otherwise, overtaking behavior is not permitted. This paper considers the situation in that USV is not allowed to overtake, and it has to follow the vessel ahead at a low speed. Hence, the speed is optimized to avoid collisions with the vessel ahead.

3.3.3 CBF design for avoiding waterway boundaries

The boundaries of the waterway are represented by two straight lines, denoted by L_{ij} (Figure 4), and their expressions are defined as follows:

$$a_{ij}x + b_{ij}y + c_{ij} = 0, \quad i = 1, 2, \dots, n, \quad j = 1, 2 \quad (51)$$

where a_{ij} , b_{ij} , and $c_{ij} \in \mathbb{R}$ are the parameters of the line.

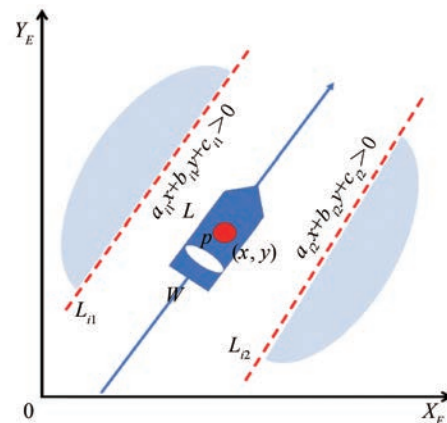


Figure 4 Schematic diagram of the waterway boundary constraints

Based on the property of (51), the area where the two straight lines are larger than zero is defined as a safety set for the USV, and the safety area \mathcal{C} can be expressed as follows:

$$\mathcal{C} = \{ p \in \mathbb{R}^2 | (a_{i1}x + b_{i1}y + c_{i1} > 0) \cap (a_{i2}x + b_{i2}y + c_{i2} > 0) \}$$

The distance between the USV and the waterway boundary is defined as follows:

$$D_{ij} = \frac{a_{ij}x + b_{ij}y + c_{ij}}{\sqrt{a_{ij}^2 + b_{ij}^2}}, \quad i = 1, 2, \dots, n, \quad j = 1, 2 \quad (52)$$

In ensuring the safety, the safety set is defined as follows:

$$\mathcal{S}_3 = \{ p \in \mathbb{R}^2 | h_{ij}(p) = D_{ij} - \frac{\sqrt{L^2 + W^2}}{2} - d_{ij} \geq 0 \} \quad (53)$$

indicating that the distance between each edge of the USV and the waterway boundaries should be larger than distance d_{ij} . By using (8), the second time derivatives of h_{ij} in (53) can be expressed as follows:

$$\ddot{h}_{ij} + \alpha_c \dot{h}_{ij} + \alpha_c^2 h_{ij} \geq 0, \quad i = 1, 2, \dots, n, \quad j = 1, 2 \quad (54)$$

and the corresponding waterway boundary constraints are expressed as follows:

$$\mathcal{U}_3(r_o) = \{ r_o | A_{ij}r_o + B_{ij}\alpha_c + C_{ij}\alpha_c^2 + M_{ij} \geq D_{ij} \} \quad (55)$$

$$i = 1, 2, \dots, n, \quad j = 1, 2$$

where

$$\begin{aligned} A_{ij} &= U_o(b_{ij} \cos(\psi + \beta) - a_{ij} \sin(\psi + \beta)) \\ B_{ij} &= a_{ij}(U_o \cos(\psi + \beta) + \hat{w}_x) \\ &\quad + b_{ij}(U_o \sin(\psi + \beta) + \hat{w}_y) \\ C_{ij} &= a_{ij}x + b_{ij}y + c_{ij} - \frac{\sqrt{(L^2 + W^2)(a_{ij}^2 + b_{ij}^2)}}{2} \\ &\quad - d_{ij}\sqrt{a_{ij}^2 + b_{ij}^2} \\ D_{ij} &= -a_{ij}\dot{U}_o \cos(\psi + \beta) - a_{ij}\dot{U}_o \sin(\psi + \beta) \\ M_{ij} &= -a_{ij}\alpha_c \tilde{w}_x - b_{ij}\alpha_c \tilde{w}_y \end{aligned}$$

and $\alpha_c \in \mathbb{R}$ is a positive constant.

3.4 Safety-certificated guidance law design

By using the safety constraints determined by CBFs, two quadratic programming problems are formulated herein to optimize the obtained guidance law in a minimal invasion way to ensure the safety of the USV. In addition, the following velocity constraints are enforced to satisfy

the following equation:

$$\begin{aligned} \underline{U} &\leq U_o \leq \bar{U} \\ \underline{r} &\leq r_o \leq \bar{r} \end{aligned} \quad (56)$$

where $\underline{U} \in \mathbb{R}$, $\bar{U} \in \mathbb{R}$, $\underline{r} \in \mathbb{R}$, and $\bar{r} \in \mathbb{R}$ are constants.

The optimized velocity U_o is obtained by solving the following quadratic programming problem:

$$\begin{aligned} U_o &= \arg \min_{U_o \in \mathbb{R}} J(U_o) = |U_o - U_{\text{cmd}}|^2 \\ \text{s.t. } A_{km}U &\geq D_{km} - B_{km}\alpha_m - M_{km} \\ k &= 1, 2, \dots, M_2, \quad \underline{U} \leq U_o \leq \bar{U} \end{aligned} \quad (57)$$

Similarly, the optimized yaw rate r_o is obtained as follows:

$$\begin{aligned} r_o &= \arg \min_{r_o \in \mathbb{R}} J(r_o) = |r_o - r_{\text{cmd}}|^2 \\ \text{s.t. } A_{ks}r_o &\geq D_{ks} - C_{ks}\alpha_s^2 - B_{ks}\alpha_s - M_{ks}, \\ k &= 1, 2, \dots, M_1 \\ A_{ij}r_o &\geq D_{ij} - C_{ij}\alpha_c^2 - B_{ij}\alpha_c - M_{ij}, \\ j &= 1, 2, \quad \underline{r} \leq r_o \leq \bar{r} \end{aligned} \quad (58)$$

The safety of the USV system is given by the following lemma.

Lemma 6. Given an under-actuated USV with dynamics (9), if the optimal control signal $U_o \in \mathcal{U}_2$ and $r_o \in \mathcal{U}_1 \cap \mathcal{U}_3$ for the USV, and $p(t_0) \in \mathcal{S}_1 \cap \mathcal{S}_2 \cap \mathcal{S}_3$, $\forall t > t_0$, then, the USV system is ISSf.

Proof: The set $\mathcal{S} = \mathcal{S}_1 \cap \mathcal{S}_2 \cap \mathcal{S}_3$ is forward invariant by using the optimal control signal $U_o \in \mathcal{U}_2$ and $r_o \in \mathcal{U}_1 \cap \mathcal{U}_3$; that is, the set \mathcal{S} is ISSf. Therefore, if the initial position of the USV satisfies $p(t_0) \in \mathcal{S}_1 \cap \mathcal{S}_2 \cap \mathcal{S}_3$, then $p(t)$ will stay in $\mathcal{S}_1 \cap \mathcal{S}_2 \cap \mathcal{S}_3$. Therefore, the USV system is ISSf.

The stability and safety of the proposed system of USV are given by the following theorem.

Theorem 1. Consider a USV with dynamics (9), the ESO (19), safety constraints (47), (50), and (55), optimal surge velocity (57), and optimal yaw rate (58). All error signals in the closed-loop system are uniformly and ultimately bounded, and the USV system is ISSf.

Proof: Based on Lemma 6, the USV will not violate the safety requirements; that is, the safety objectives (16), (17), and (18) are achieved. Lemma 3 shows that the tracking error signal E_2 is bounded; that is, there exists a positive constant such that the geometric objective (15) is achieved.

4 Simulation of a USV in the yangtze river

Consider a motion scenario that a USV runs in the waterway of the Yangtze River. Moreover, consider one sta-

tionary obstacle and one moving obstructive vehicle running at a low velocity ahead of the USV.

In the simulation, the length and width of the USV are set as $L = 1.5$ and $W = 0.4$, respectively. The ocean currents are set as $w_s = -0.5$ and $w_e = 0.2$. The velocity constraints are given as $\underline{U} = 0$, $\bar{U} = 1$, $\underline{r} = -0.5$, and $\bar{r} = 0.5$. The initial position of the USV is $\mathbf{p}(0) = [2, 72.5]^T$. The desired straight lines are determined by three waypoints, that is, $\mathbf{p}_{1d} = [0, 72.5]^T$, $\mathbf{p}_{2d} = [21.6, 60.0]^T$, and $\mathbf{p}_{3d} = [88.0, 0]^T$. The parameters of the four waterway boundaries are $119x + 195y - 13494 = 0$, $-152x - 233y + 17800.2 = 0$, $573x + 635y - 47559 = 0$, and $-566x - 662y - 53852.8 = 0$. The stationary obstacle locates $\mathbf{p}_{1s} = [34.0, 50.0]^T$. The obstructive vehicle moves at a speed of 0.7 m/s on the route. The safe distances are set as follows:

$d_{11} = d_{12} = d_{21} = d_{22} = d_{31} = d_{32} = 2$, $d_{1s} = 3$, and $d_{1m} = 20$. The ESO parameters are selected as $k_{s1} = 1$, $k_{e1} = 1$, $k_{s2} = 0.25$, and $k_{e2} = 0.25$. The LOS guidance parameters are selected as $k_u = 1$, $\Delta_u = 0.5$, $\Delta_\psi = 8$, $k_r = 0.5$, and $\Delta_r = 0.3$. The CBF parameters are set as $\alpha_c = 0.5$, $\alpha_s = 0.45$, and $\alpha_m = 0.05$. In the simulation, the quadratic optimization problem is solved by the built-in Python toolbox cvxpy.

The simulation results are provided in Figures 5–9. Figure 5(a) shows the simulation results of the proposed guidance method. Compared with Figure 5(b), safety is ensured; that is, the collisions with waterway boundaries and obstacles are prevented by using the proposed CBF-based guidance method. Compared with Figure 5(c), the USV can accurately track the desired route by using the proposed ESO-based guidance method. Figure 6 shows the tracking errors of the USV in the s and e directions. Based on the error shown in the s direction, the proposed method and the method without ESO can reduce the velocity when encountering a moving obstacle. Based on the error in the e direction, the error cannot be eliminated by using the method without ESO as the effect of unknown ocean currents. Figure 7 shows the estimation performance of the ocean current ESO. The unknown constant ocean currents are estimated accurately. Figure 8 shows the yaw rate tracking performance. The commanded yaw rate is optimized at 0 – 20 s and 70 – 80 s to ensure the collision avoidance of waterway boundaries and obstructive vehicles, respectively. The peak at 50 s is induced by the change of the desired straight-line route. Figure 9 shows the surge velocity tracking performance. The peak at 50 s is also induced by the change of the desired straight-line route. Considering the role of CBF, the USV can decelerate after 130 s because of the presence of a moving vessel in front of it. Figure 10 shows the quadratic programming time for the surge and yaw directions. The optimization time is less than the sampling time ΔT in each cycle, which can be accomplished in each cycle. Figure 11 shows the ratio of the quadratic programming time to the

total execution time in each cycle. As shown in the figure, optimization occupies more than 90% of the total execution time in each cycle.

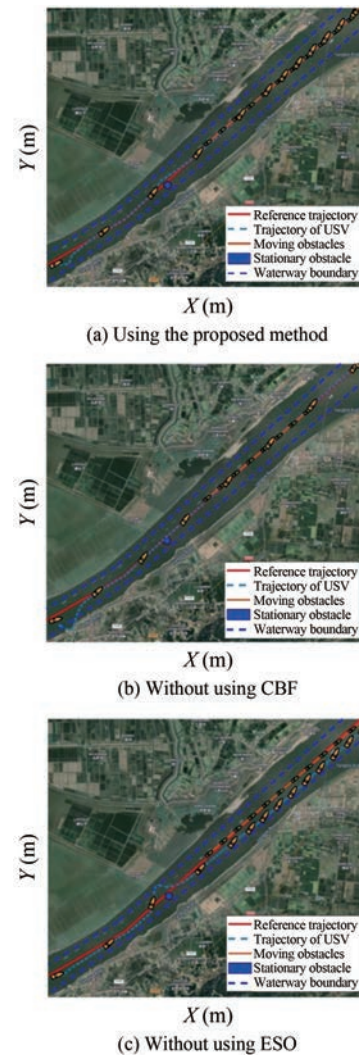


Figure 5 USV trajectory

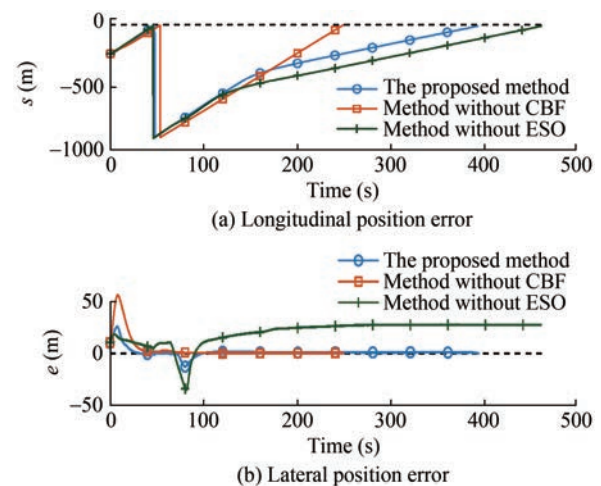


Figure 6 Comparison of position errors using three methods

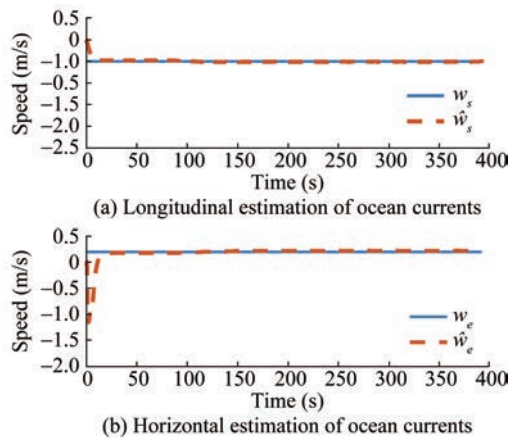


Figure 7 Estimation performance of the ESO

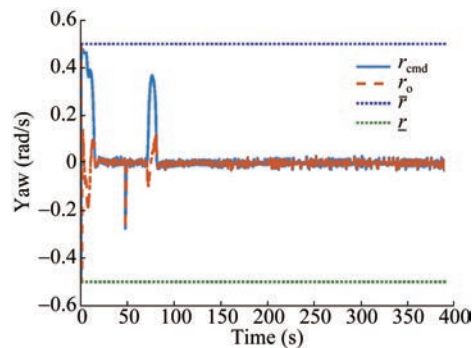


Figure 8 Commanded yaw rate and optimized yaw rate command

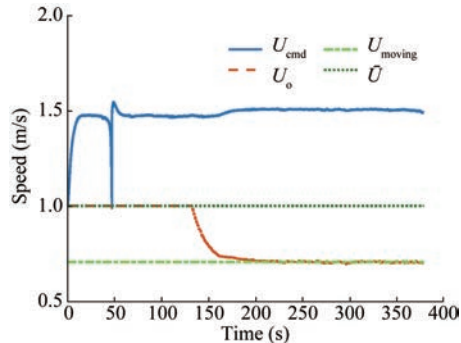


Figure 9 Commanded surge speed and optimized surge speed command

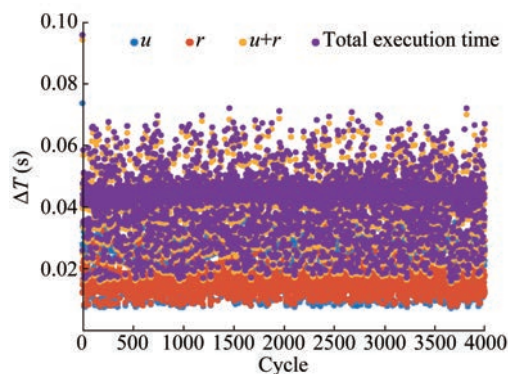


Figure 10 Quadratic programming time

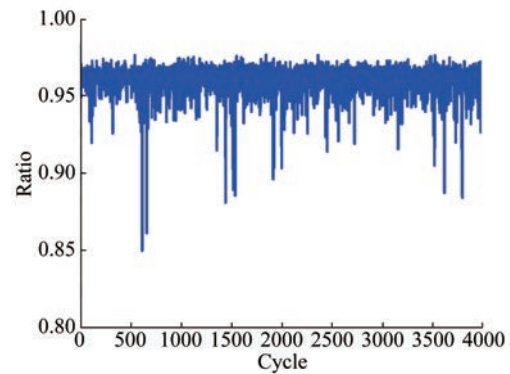


Figure 11 Ratio of the quadratic programming time to the total execution time in each cycle

5 Conclusion

This paper presents a safety-certified straight-line following of a USV in a constrained water region with waterway boundaries and stationary/moving obstacles. An ESO is designed to estimate external environmental disturbances. Design guidance laws based on the principle of LOS, and compensate for external disturbances based on the ESO results. Then, a quadratic programming problem is formulated such that the safety constraints encoded by CBFs and velocity constraints are satisfied. Therefore, all tracking errors of the closed-loop system are uniformly and ultimately bounded, and the system is ISSf. The simulation results substantiate the effectiveness of the proposed safety-certified straight-line following guidance method. In future work, the USV dynamic model must be considered, and the antidisturbance safe-certificated path following control must be investigated for a USV in a constrained water region.

Funding Supported by the National Key R&D Program of China under Grant No. 2022ZD0119902, the National Natural Science Foundation of China under Grant No. 51979020, the Top-notch Young Talents Program of China under Grant No. 36261402, the Dalian High-level Talents Innovation Support Program under Grant No. 2022RQ010, the Liaoning Revitalization Talents Program under Grant No. XLYC2007188, the Natural Science Foundation of Fujian Province under Grant No. 2022J01131710, the Postdoctoral Research Foundation of China under Grant No. 2022M720619, and in part by the Fundamental Research Funds for the Central Universities 3132023107.

Competing interest Zhouhua Peng is an editorial board member for the Journal of Marine Science and Application and was not involved in the editorial review, or the decision to publish this article. All authors declare that there are no other competing interests.

References

Abdurahman B, Savvaris A, Tsourdos A (2019) Switching LOS guidance with speed allocation and vertical course control for

- path-following of unmanned underwater vehicles under ocean current disturbances. *Ocean Engineering* 182: 412-426. <https://doi.org/10.1016/j.oceaneng.2019.04.021>
- Aguiar AP, Hespanha JP (2007) Trajectory-tracking and pathfollowing of underactuated autonomous vehicles with parametric modeling uncertainty. *IEEE Transactions on Automatic Control* 52(8): 1362-1379. DOI: 10.1109/TAC.2007.902731
- Ames AD, Xu X, Grizzle JW, Tabuada P (2017) Control Barrier function based quadratic programs for safety critical systems. *IEEE Transactions on Automatic Control* 62(8): 3861-3876. DOI: 10.1109/TAC.2016.2638961
- Belleter D, Maghenem MA, Paliotta C, Pettersen K Y (2019) Observer based path following for underactuated marine vessels in the presence of ocean currents: A global approach. *Automatica* 100: 123-134. <https://doi.org/10.1016/j.automatica.2018.11.008>
- Breivik M, Hovstein VE, Fossen TI (2008) Straight-line target Tracking for unmanned surface vehicles. *Modeling, Identification and Control: A Norwegian Research Bulletin* 29(4): 131-149. DOI: 10.4173/mic.2008.4.2
- Campbell S, Naeem W, Irwin GW (2012) A review on improving the autonomy of unmanned surface vehicles through intelligent collision avoidance manoeuvres. *Annual Reviews in Control* 36(2): 267-283. <https://doi.org/10.1016/j.arcontrol.2012.09.008>
- Caharija W, Pettersen KY, Bibuli M, Calado P, Zereik E, Braga J, Gravdahl JT, Sørensen AJ, Milovanović M, Bruzzone G (2016) Integral line-of-sight guidance and control of underactuated marine vehicles: Theory, simulations, and experiments. *IEEE Transactions on Control Systems Technology* 24(5): 1623-1642. DOI: 1109.2015 / TCST.2504838
- Chen YY, Wei P (2014) Coordinated adaptive control for coordinated path-following surface vessels with a time-invariant orbital velocity. *Journal of Automatica Sinica* 1(4): 337-346. DOI: 10.1109/JAS.2014.7004662
- Daş E, Murray RM (2022) Robust safe control synthesis with disturbance observer-based control barrier functions. 2022 IEEE 61st Conference on Decision and Control (CDC), 5566-5573. <https://doi.org/10.48550/arXiv.2201.05758>
- Deng Y, Zhang X, Zhang G (2020) Line-of-sight-based guidance and adaptive neural path-following control for sailboats. *Ocean Engineering* 45(4): 1177-1189. DOI: 10.1109/JOE.2019.2923502
- Fossen TI, Lekkas AM (2017) Direct and indirect adaptive integral line-of-sight path-following controllers for marine craft exposed to ocean currents. *International Journal of Adaptive Control and Signal Processing* 4: 445-463. <https://doi.org/10.1002/acs.2550>
- Fossen TI, Pettersen KY (2014) On uniform semiglobal exponential stability (USGES) of proportional line-of-sight guidance laws. *Automatica* 50(11): 2912-2917. DOI: 10.1016/j.automatica.2014.10.018
- Gu N, Wang D, Peng ZH, Wang J, Han QL (2022) Disturbance observers and extended state observers for marine vehicles: A survey. *Control Engineering Practice* 123: 105158. <https://doi.org/10.1016/j.conengprac.2022.105158>
- Gu N, Wang D, Peng ZH, Wang J (2021) Safety-critical containment maneuvering of underactuated autonomous surface vehicles based on neurodynamic optimization with control barrier functions. *IEEE Transactions on Neural and Learning Systems*, 1-14. DOI: 10.1109/TNNLS.2021.3110014
- Gu N, Wang D, Peng ZH, Wang J, Han QL (2023) Advances in line-of-sight guidance for path following of autonomous marine vehicles: An overview. *IEEE Transactions on Systems, Man, and Cybernetics: Systems* 53(1): 12-28. DOI: 10.1109/TSMC.2022.3162862
- He W, Yin Z, Sun C (2017) Adaptive neural network control of a marine vessel with constraints using the asymmetric barrier lyapunov function. *IEEE Transactions on Cybernetics* 47(7): 1641-1651. DOI: 10.1109/TCYB.2016.2554621
- Jiang H, Liang Y (2018) Online path planning of autonomous UAVs for bearing-only standoff multi-target following in threat environment. *IEEE Access* 6: 22531-22544. DOI: 10.1109/ACCESS.2018.2824849
- Katayama H, Aoki H (2014) Straight-line trajectory tracking control for sampled-data underactuated ships. *IEEE Transactions on Control Systems Technology* 22(4): 1638-1645. DOI: 10.1109/TCST.2013.2280717
- Khalil HK (2015) *Nonlinear control*. Pearson Education
- Kolathaya S, Ames AD (2019) Input-to-state safety with control Barrier functions. *IEEE Control Systems Letters* 3(1): 108-113. DOI: 10.1109/LCSYS.2018.2853698
- Li JJ, Xiaog XB, Yang SL (2022) Robust adaptive neural network control for dynamic positioning of marine vessels with prescribed performance under model uncertainties and input saturation. *IEEE Transactions Automation Science and Engineering* 484: 1-12. <https://doi.org/10.1016/j.neucom.2021.03.136>
- Li TS, Zhao R, Chen CLP, Fang LY, Liu C (2018) Finite-time formation control of under-actuated ships using nonlinear sliding mode control. *IEEE Transactions on Cybernetics* 48(11): 3243-3253. DOI: 10.1109/TCYB.2018.2794968
- Liu L, Wang D, Peng ZH (2017) ESO-based line-of-sight guidance law for path following of underactuated marine surface vehicles with exact sideslip compensation. *IEEE Journal of Ocean Engineering* 42(2): 477-487. DOI: 10.1109/JOE.2016.2569218
- Liu L, Wang D, Peng ZH, Wang Hao (2016) Predictor-based LOS guidance law for path following of underactuated marine surface vehicles with fast sideslip compensation. *Ocean Engineering* 124(2): 340-348. <https://doi.org/10.1016/j.oceaneng.2016.07.057>
- Lv MG, Peng ZH, Wang D, Han QL (2022) Event-triggered cooperative path following of autonomous surface vehicles over wireless network with experiment results. *IEEE Transactions on Industrial Electronics* 69(11): 11479-11489. DOI: 10.1109/TIE.2021.3120442
- Maghenem M, Belleter DJW, Paliotta C, Pettersen KY (2017) Observer based path following for underactuated marine vessels in the presence of ocean currents: a local approach. *IFAC-Papers OnLine* 50(1): 13654-13661. <https://doi.org/10.1016/j.ifacol.2017.08.2399>
- Ma Y, Hu MQ, Yan XP (2018) Multi-objective path planning for unmanned surface vehicle with currents effects. *ISA Transactions* 75: 137-156. <https://doi.org/10.1016/j.isatra.2018.02.003>
- Ma Y, Zhao YJ, Li ZX, Bi HX, Wang J, Malekian R, Sotelo M (2022) CCIBA*: An improved BA* based collaborative coverage path planning method for multiple unmanned surface mapping vehicles. *IEEE Transactions on Intelligent Transportation Systems* 23(10): 19578-19588. DOI: 10.1109/TITS.2022.3170322
- Ma Y, Zhao YJ Incecik Atilla, Yan XP, Wang YL, Li ZX (2021) A collision avoidance approach via negotiation protocol for a swarm of USVs. *Ocean Engineering* 224: 108713. <https://doi.org/10.1016/j.oceaneng.2021.108713>
- Meng W, Guo G, Liu Y (2012) Robust adaptive path following for underactuated surface vessels with uncertain dynamics. *Journal of Marine Science and Application* 11(2): 244-250. <https://doi.org/10.1007/s11804-012-1129-y>
- Molnar TG, Cosner RK, Singletary AW, Ubellacker W, Ames AD (2022) Model-free safety-critical control for robotic systems. *Robotics and Automation Letters* 7(2): 944-951. DOI: 10.1109/LRA.2021.3135569
- Paliotta C, Lefeber E, Pettersen KY, Pinto J, Costa M, de Figueiredo Borges de Sousa JT (2019) Trajectory tracking and path

- following for underactuated marine vehicles. *IEEE Transactions on Control Systems Technology* 27(4): 1423-1437. DOI: 10.1109/TCST.2018.2834518
- Peng ZH, Wang C, Yin Y, Wang J (2023) Safety-certified constrained control of maritime autonomous surface ships for automatic berthing. *IEEE Transactions on Vehicular Technology*, early access. DOI: 10.1109/TVT.2023.3253204
- Peng ZH, Wang D, Wang J (2021) Data-driven adaptive disturbance observers for model-free trajectory tracking control of maritime autonomous surface ships. *IEEE Transactions on Neural Networks and Learning Systems* 32(12): 5584-5594. DOI: 10.1109/TNNLS.2021.3093330
- Peng ZH, Wang J, Han QL (2019) Path-following control of autonomous underwater vehicles subject to velocity and input constraints via neurodynamic optimization. *IEEE Transactions on Industrial Electronics* 66(11): 8724-8732. DOI: 10.1109/TIE.2018.2885726
- Peng ZH, Wang J, Wang D, Han QL (2021) An overview of recent advances in coordinated control of multiple autonomous surface vehicles. *IEEE Transactions on Industrial Informatics* 17(2): 732-745. DOI: 10.1109/TII.2020.3004343
- Qu Y, Xu HX, Yu WZ, Feng H, Han X (2017) Inverse optimal control for speed-varying path following of marine vessels with actuator dynamics. *Journal of Marine Science and Application* 16(2): 225-236. <https://doi.org/10.1007/s11804-017-1410-1>
- Shi Y, Shen C, Fang H, Li H (2017) Advanced control in marine mechatronic systems: A survey. *IEEE Transactions on Mechatronics* 22(3): 1121-1131. DOI: 10.1109/TMECH.2017.2660528
- Skjetne R, Fossen TI, Kokotovic PV (2005) Adaptive maneuvering, with experiments, for a model ship in a marine control laboratory. *Automatica* 41(2): 289-298. DOI: 10.1016/j.automatica.2004.10.006
- Veremey EI (2014) Dynamical correction of control laws for marine ships accurate steering. *Journal of Marine Science and Application* 13(2): 127-133. <https://doi.org/10.1007/s11804-014-1250-1>
- Wang NJ, Liu HB, Yang WH (2012) Path-tracking control of a tractor-aircraft system. *Journal of Marine Science and Application* 11(4): 512-517. <https://doi.org/10.1007/s11804-012-1162-x>
- Wang Y, Tong H, Fu M (2019) Line-of-sight guidance law for path following of amphibious hovercrafts with big and timevarying sideslip compensation. *Ocean Engineering* 172: 531-540. <https://doi.org/10.1016/j.oceaneng.2018.12.036>
- Wang Z, Yang SL, Xiang XB, Antonio V, Nikola M, Dula N (2021) Cloud-based mission control of USV fleet: Architecture, implementation and experiments. *Control Engineering Practice* 106: 104657. <https://doi.org/10.1016/j.conengprac.2020.104657>
- Wu F, Wang XG, Liu T (2020) An empirical analysis of high-quality marine economic development driven by marine technological innovation. *Journal of Coastal Research* 115: 465-468. <https://doi.org/10.2112/JCR-SI115-129.1>
- Wu WT, Peng ZH, Liu L, Wang D (2022a) A general safety-certified cooperative control architecture for interconnected intelligent surface vehicles with applications to vessel train. *IEEE Transactions on Intelligent Vehicles* 7(3): 627-637. DOI: 10.1109/TIV.2022.3168974
- Wu WT, Peng ZH, Wang D, Liu L, Gu N (2022b) Anti-disturbance leader-follower synchronization control of marine vessels for underway replenishment based on robust exact differentiators. *Ocean Engineering* 248: 110686. <https://doi.org/10.1016/j.oceaneng.2022.110686>
- Wu WT, Peng ZH, Wang D, Liu L, Han QL (2021) Network-based line-of-sight path tracking of underactuated unmanned surface vehicles with experiment results. *IEEE Transactions on Cybernetics* 52(10): 10937-10947. DOI: 10.1109/TCYB.2021.3074396
- Yu C, Liu C, Lian L, Xiang X, Zeng Z (2019a) ELOS-based path following control for underactuated surface vehicles with actuator dynamics. *Automatica* 187: 106139. <https://doi.org/10.1016/j.oceaneng.2019.106139>
- Yu C, Xiang X, Wilson PA, Zhang Q (2020) Guidance-error-based robust fuzzy adaptive control for bottom following of a flightstyle AUV with saturated actuator dynamics. *IEEE Transactions on Cybernetics* 50(5): 1887-1899. DOI: 10.1109/TCYB.2018.2890582
- Yu Y, Guo C, Yu H (2019b) Finite-time PLOS-based integral sliding mode adaptive neural path following for unmanned surface vessels with unknown dynamics and disturbances. *IEEE Trans Automation Science and Engineering* 16(4): 1500-1511. DOI: 10.1109/TASE.2019.2925657
- Zereik E, Bibuli M, Miskovic N, Ridao P, Pascoal A (2018) Challenges and future trends in marine robotics. *Annual Reviews in Control* 46: 350-368. <https://doi.org/10.1016/j.arcontrol.2018.10.002>
- Zhang Q, Zhang JL, Chemori A, Xiang XB (2018) Virtual submerged floating operational system for robotic manipulation. *Complexity* 9528313: 1076-2787. <https://doi.org/10.1155/2018/9528313>
- Zheng ZW, Huang Y, Xie L (2018) Error-constrained LOS path following of a surface vessel with actuator saturation and faults. *IEEE Transactions on Systems, Man, and Cybernetics: Systems* 48(10): 1794-1805. DOI: 10.1109/TSMC.2017.2717850
- Zheng ZW (2020) Moving path following control for a surface vessel with error constraint. *Automatica* 118: 109040. <https://doi.org/10.1016/j.automatica.2020.109040>